Sensors & Actuators: B. Chemical 299 (2019) 126992

Contents lists available at ScienceDirect

Sensors and Actuators B: Chemical

journal homepage: www.elsevier.com/locate/snb

Doping effects of ZnO quantum dots on the sensitive and selective detection of acetylene for dissolved-gas analysis applications of transformer oil

Min Sun Park[1], Jun Ho Lee[1], Yunji Park, Ran Yoo, Seungryol Park, Hwaebong Jung, Wonkyung Kim, Hyun-Sook Lee*, Wooyoung Lee*

Department of Materials Science and Engineering, Yonsei University, 50 Yonsei-ro, Seodaemun-gu, Seoul, 03722, Republic of Korea

ARTICLE INFO

Keywords:
Acetylene gas sensor
ZnO
Quantum dots
Transformer oil
Dissolved gas analysis
Gas chromatography

ABSTRACT

We report on the doping effect on the sensing properties of ZnO quantum dots (QDs) for the detection of acetylene. We found that In-doped ZnO (IZO) QDs exhibited a better sensing performance to 10 ppm acetylene than undoped ZnO (ZO) QDs and Al-doped ZnO (AZO) QDs. The higher sensing response of IZO QDs can be attributed to a greater number of reactive sites for detecting acetylene, which is likely to originate from the increased number of oxygen vacancies, and the larger optical band gap and surface area of IZO. This is due to a higher valence dopant and a smaller particle size. The sensing properties of IZO QDs to 10 ppm acetylene was also found to be superior to previously reported acetylene sensors that are based on semiconducting metal oxides. Furthermore, we demonstrated that 10 ppm of acetylene can be selectively detected in air within ~100 s using a recently developed miniaturized gas chromatography (GC) integrated with the IZO QDs sensor. In addition, we found that the device can detect the major fault gases of hydrogen and acetylene separately within ~100 s. Our study demonstrates that the device can be utilized in the GC-based on-line dissolved gas analysis to detect small amounts of acetylene gas in transformer oil.

1. Introduction

Monitoring transformer oils to detect dissolved gas is an important indicator for diagnosing failure and predicting the life time of transformers [1,2]. When a fault occurs, the insulation oil or cellulose starts to decompose and to produce by-product gases, which dissolve into the transformer oil. Mainly, such fault gases are hydrogen (H_2), hydrocarbons (CH_4, C_2H_2, C_2H_4, C_2H_6), and carbon oxides (CO, CO_2) [1]. The amounts and types of the fault gases vary depending on the type of fault, i.e. partial discharge (corona), overheating (pyrolysis), and arcing [1–3]. Among the fault gases, acetylene (C_2H_2) is one of the most dangerous gases that should be monitored in transformer oils. This is because it characteristically evolves during arc discharge, which can lead to catastrophic transformer accidents. Moreover, an accurate detection of acetylene gas is required because it has the lowest safety limit of all fault gases [2].

Various methods have been introduced to analyze the fault gases in transformer oils. One of the most widely used diagnostic tools is dissolved gas analysis (DGA), which represents the single great indicator of a transformer's overall condition [3–5]. A major detection method is gas chromatography (GC) using a sample of oil extracted from the transformer. It is highly reliable, but does not allow to detect dissolved gases in real time because a minimum analysis period ranging between two hours to more than a full day is required [6]. Lately, a range of spectroscopic methods have been applied to detect fault gases such as laser calorimetry [7], photoacoustic [8], optical fiber [9], and tunable diode laser absorption spectroscopy [10]. However, these methods exhibit a lower sensitivity and higher detection limit for dissolved gases owing to mechanical vibrations and a significant background signal [10].

In order to continuously and accurately monitor dissolved gases in-situ, GC-based on-line DGA monitors have been developed [11]. The on-line DGA systems both extract and detect gases. For the gas extraction, a number of gas separation methods are available such as vibration degassers, and hollow fiber and polymer membranes [12]. Membrane-based gas separations are promising technologies for gas extraction in transformer oil. Compared to the traditional vacuum method, it enables a more continuous operation and lower maintenance costs. For a successful gas separation, only gases but not oil should be able to freely pass through a dense polymeric membrane [13]. Various

* Corresponding authors.
E-mail addresses: h-slee@yonsei.ac.kr (H.-S. Lee), wooyoung@yonsei.ac.kr (W. Lee).
[1] These authors contributed equally.

https://doi.org/10.1016/j.snb.2019.126992
Received 17 May 2019; Received in revised form 30 July 2019; Accepted 16 August 2019
Available online 17 August 2019
0925-4005/

studies have been conducted aiming to find appropriate membrane materials with good chemical and thermal stability as well as high gas permeability [13].

In addition to the development of effective techniques for acetylene gas detection, many efforts have also focused on the development of sensitive sensing materials [8–10]: Ni-doped ZnO nanofibers [14], NiO/SnO_2 heterostructures [15], Ag-loaded ZnO-reduced graphene oxide (rGO) hybrids [16], Ag-loaded vertical ZnO nanorod arrays [17], SnO_2/rGO nanocomposites [18], Pt/ZnO thick films [19] etc. In particular, ZnO has become a promising candidate for acetylene sensing owing to its low cost, simple preparation, high chemical and thermal stability, and favorable sensing properties. The performance of ZnO-based sensors has been improved by controlling the structure and morphologies [20], doping of transition metals [21,22], and loading of noble metals [23,24]. Furthermore, quantum-sized ZnO nanoparticles may be able to boost the sensing performance [25].

In a recent study, we successfully synthesized ZnO quantum dots (QDs) using a wet chemical method. We found that the ZnO QD-based sensor exhibited an excellent sensing performance for various gases such as acetone [26], 2-chloroethyl ethyl sulfide (2-CEES) [27], and isoprene [28]. Furthermore, we have developed a miniaturized gas chromatographic column (mini-GC) integrated with a ZnO QD-based sensor. Using this device, we achieved a selective detection of target gases, such as acetone [26] and isoprene [28] in human breath and 2-CEES in a mixture of interfering gases (NH_3, NO, and CO) [27]. As discussed above, it is very important to accurately and selectively detect low concentrations of acetylene gas within the various fault gases dissolved in the transformer oil to diagnose arcing faults in the transformer. However, this has not yet been reported using metal-oxide semiconductor-based sensors. In this regard, a study of the sensing abilities of ZnO QDs for sensitive and selective detection of acetylene is valuable.

In this work, we investigate the doping effect on the sensing properties of ZnO QDs for the detection of acetylene. We show that doping of ZnO QDs results in a smaller crystallite size and reduced crystallinity, and gives rise to a modification of the oxidation and electronic states that affect the sensing performance. We demonstrate the high sensitivity and selectivity of a mini-GC integrated with ZnO QDs for detection of acetylene in air. This device would be suitable to utilize in a GC-based on-line DGA, which detects the extracted gases from oil by a membrane type filter, and allow for real-time monitoring to diagnose the failure of a transformer.

2. Materials and methods

2.1. Synthesis of ZnO quantum dots

Undoped ZnO quantum dots (ZO QDs) and Al- and In-doped ZnO quantum dots (AZO QD and IZO QD, respectively) were synthesized by a wet-chemical method described in detail in our previous reports [26]. Briefly, zinc acetate dihydrate ($Zn(CH_3COO)_2{\cdot}2H_2O$, Sigma Aldrich) was dissolved in N, N-Dimethylmethanamide (C_3H_7NO, DMF) to form a 0.1 M ZnO precursor solution. It was then mixed with a 0.3 M solution of tetramethylammonium hydroxide ($(CH_3)4NOH{\cdot}5H_2O$, TMAH, Sigma Aldrich) in methanol by stirring at 30 °C for 1 h. After stirring, the suspended nanoparticles were centrifuged and cleaned using acetone. The final ZnO QDs were dispersed in methanol. For synthesizing doped ZnO QDs, an Al precursor ($Al(O_2CCH_3)_3$, Alfa Aesar) and an In precursor ($InCl_3$, Sigma Aldrich) were added to the Zn precursor solution to obtain AZO and IZO QDs with a doping concentration of 1 at%, respectively. This specific doping concentration was selected because we previously found it to exhibit the best sensing properties for Al-doped ZnO nanoparticles [22].

2.2. Characterization

The surface morphology and particle size of the as-synthesized ZnO QDs were investigated by transmission electron microscopy (TEM, JEOL JEM ARM 200 F). The structural phases were identified by X-ray diffraction (XRD, Ultima IV/ME 200DX, Rigaku) with Cu Kα radiation. The chemical bonding state of the pure and doped ZnO QDs were investigated using a Fourier transform infrared (FTIR) spectrometer (Perkin-Elmer®) within the range of 4000 to 400 cm^{-1}. The analysis of surface elements was performed by X-ray photoelectron spectroscopy (XPS, K-alpha Thermo VG). The electronic structure of the samples was examined using a ultraviolet–visible spectroscopy (UV–vis, V650 JASCO) in the wavelength range of 200–800 nm.

2.3. Fabrication of sensor devices

To fabricate the sensor device, interdigitated Pt electrodes were patterned on a SiO_2 substrate (8.5 mm × 8.5 mm) for a tube furnace system and on an Al_2O_3 substrate (0.5 mm × 0.25 mm) for a mini-GC system. A Cr interlayer was used to provide a good contact of the Pt layer on the substrate. The Pt (100 nm) and Cr (20 nm) layers were deposited on the substrate by a DC magnetic sputtering system. For the fabrication of ZnO QD sensors, the prepared ZnO QD solution was dropped on the interdigitated Pt electrode and dried at 90 °C. Subsequently, we annealed the sensors at 600 °C for 30 min to remove the remaining solvent and to improve the sensor stability.

2.4. Gas sensing measurements

The gas sensing measurements were performed inside a chamber in a tube furnace system having mass flow controllers (MFCs). The acetylene concentration was adjusted in an air-balanced gas by varying the gas flow rates on the MFCs. The sensing properties of the pure and doped ZO QDs were measured using a system equipped with a nanovoltmeter (Keithley 2182) and a current source (Keithley 6220). A constant current of 10 nA was supplied for a time interval of 1 s. The operating temperature of the sensor was controlled using the temperature controller of the tube furnace. The sensing measurements of the target gas were performed at various operating temperatures in the range of 300–500 °C. The sensing performance was tested for various acetylene concentrations (0.1–10 ppm).

We also tested the selective sensing performance of the ZnO-based QDs using our recently developed mini-GC system. The method of manufacturing the mini-GC incorporating ZnO QDs and the sensing process of the mini-GC device are described in detail in our previous reports [26,27]. The working temperature of the sensor was controlled by applying a voltage through patterned Pt electrodes on the backside of the Al_2O_3 substrate.

3. Results and discussion

In order to characterize the morphologies and phases of the as-synthesized QD samples, we used high-resolution TEM and XRD. The TEM images indicate that the particles of all QD samples are almost spherical in shape and clustered together, as shown in our previous study [26]. However, we found that the QD particles slightly vary in their average size: > 5 nm for ZO, ~ 4 nm for AZO, and ~ 3.6 nm for IZO (Fig. 1(a)). The XRD patterns of the ZO, AZO, and IZO QDs reveal the crystal structure of a hexagonal wurtzite phase (ICDD: #98-000-0483) without any secondary or impurity phases (Fig. 1(b)). We observed that the main (101) diffraction peak shifted to higher angles for AZO and to lower angles for IZO as compared to the undoped ZO (inset of Fig. 1(b)). These shifts likely originate from the substitutions of Zn^{2+} (ionic radius of 0.74 Å) by the smaller Al^{3+} (0.54 Å) and the larger In^{3+} (0.81 Å) at the lattice points of the ZnO, respectively [29–31]. All samples showed broadening main (110), (002), and (101) peaks, which

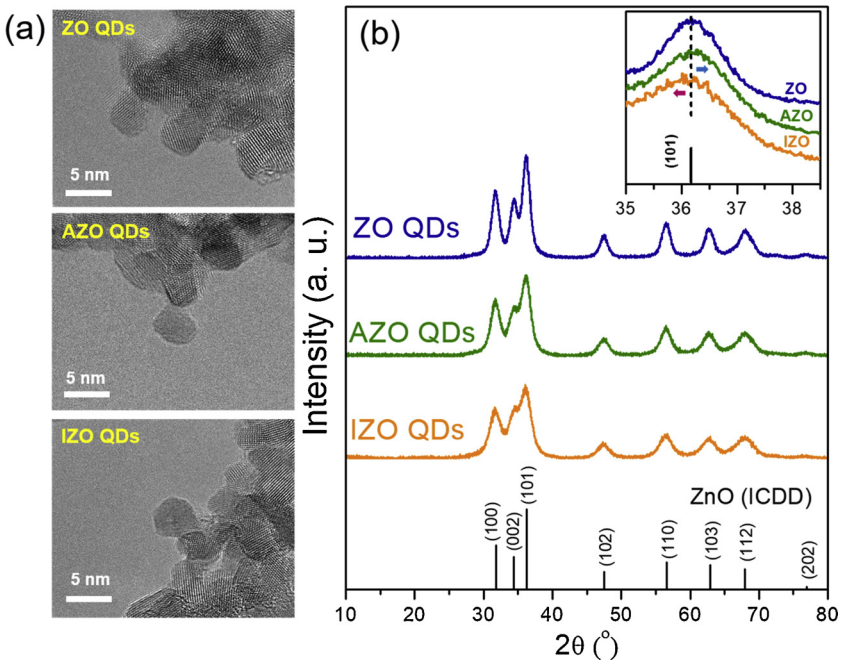

Fig. 1. (a) TEM images of the filter-collected and isolated undoped ZnO (ZO), Al-doped ZnO (AZO), and In-doped ZnO (IZO) QDs; (b) XRD patterns of ZO (blue), AZO (green), and IZO QDs (orange). The vertical lines at the bottom correspond to the standard XRD pattern of hexagonal wurtzite-type ZnO (ICDD: # 98-000-0483). The inset shows a zoom into the (101) peak of the samples. The red and light blue arrows indicate the peak shift for the IZO and AZO samples, respectively. (For interpretation of the references to colour in this figure legend, the reader is referred to the web version of this article).

appears to be more pronounced in the doped QDs, especially for IZO. This is likely owing to the small crystallite sizes. The doped QDs also exhibited a reduced peak intensity, which indicates that the crystallinity is deteriorated by the doping elements.

We estimated the average crystallite sizes of the samples from the (101) peak using Scherrer's equation to ~ 5.5 nm for ZO, ~ 4.3 nm for AZO, and ~ 3.7 nm for IZO. These are consistent with the results of the TEM analysis. Al doping reduces the crystallite size of the QDs because the smaller ionic radius of Al^{3+} compared to Zn^{2+} decreases the unit cell volume. However, the crystallite size of IZO is even smaller than of AZO although the ionic radius of In^{3+} is larger than of Zn^{2+}. We presume that this is because the larger ion radius induces a higher compressive stress in the crystal structure [32,33].

In order to investigate whether the dopants Al and In have been completely incorporated into the ZnO lattice, we obtained the chemical bonding characteristics of the QD samples using FTIR spectroscopy. The peaks in the FTIR transmission spectra of the ZO, AZO and IZO QDs are largely similar (Fig. 2(a)). The broad absorption band at ~3421 cm^{-1} can be attributed to the O—H stretching vibration of water molecules that are absorbed onto the surface of the nanocrystalline powders [34]. The peaks centered at ~2350 cm^{-1} and ~1445 cm^{-1} arose from the absorption of atmospheric CO_2 [35]. We also observed the strong asymmetric stretching vibration mode of C═O at ~1622 cm^{-1} and the symmetric stretching of C—O at ~1480 cm^{-1} and ~1380 cm^{-1} [36]. We attribute the peak around 1000 cm^{-1} to the C—O—C bond due to ambient environment [36].

The spectra of the samples differ, however, in the range from 800–400 cm^{-1} (Fig. 2(b)). In the AZO and IZO samples, we observed a tiny peak at about 683 cm^{-1}, which is absent in ZO. We assign this to a fingerprint of the Al–O and In–O bonds [30,34]. A highly intense and broad absorption band was observed in the range of 600–400 cm^{-1} corresponding to the stretching vibration of the Zn–O bond, which

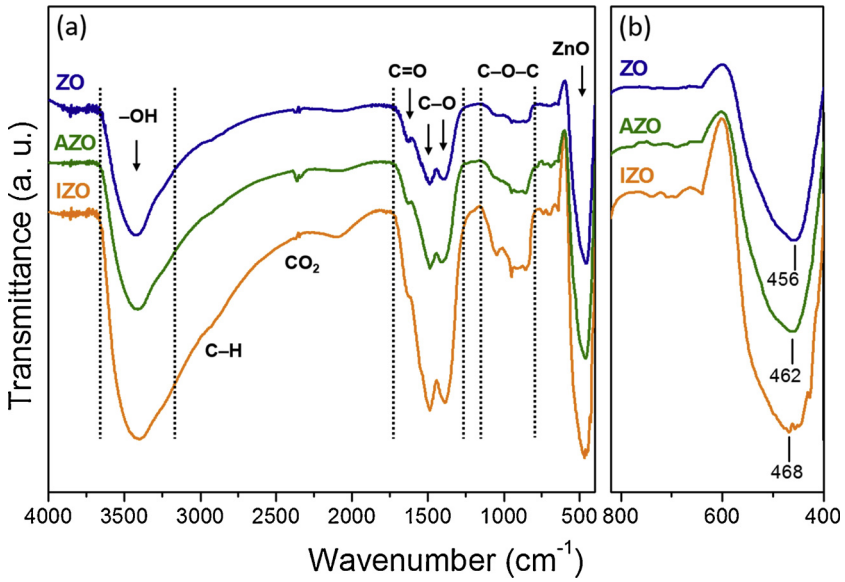

Fig. 2. FTIR spectra of ZO (blue), AZO (green), and IZO QDs (orange) in the range of (a) 4000 – 400 cm^{-1} and (b) 800 – 400 cm^{-1}. (For interpretation of the references to colour in this figure legend, the reader is referred to the web version of this article).

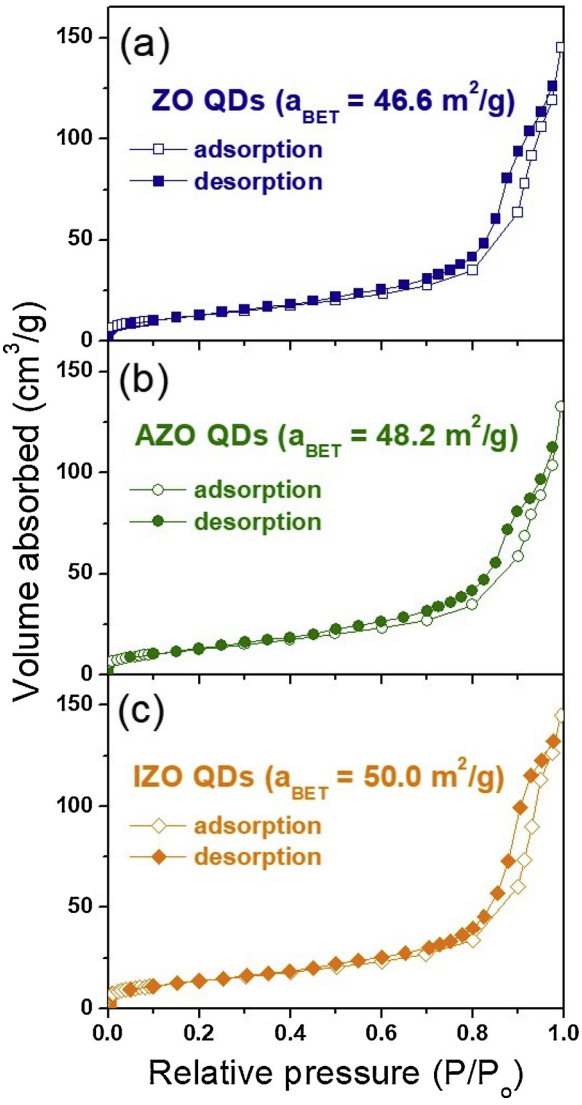

Fig. 3. N_2 adsorption–desorption isotherm of (a) ZO, (b) AZO, and (c) IZO QDs.

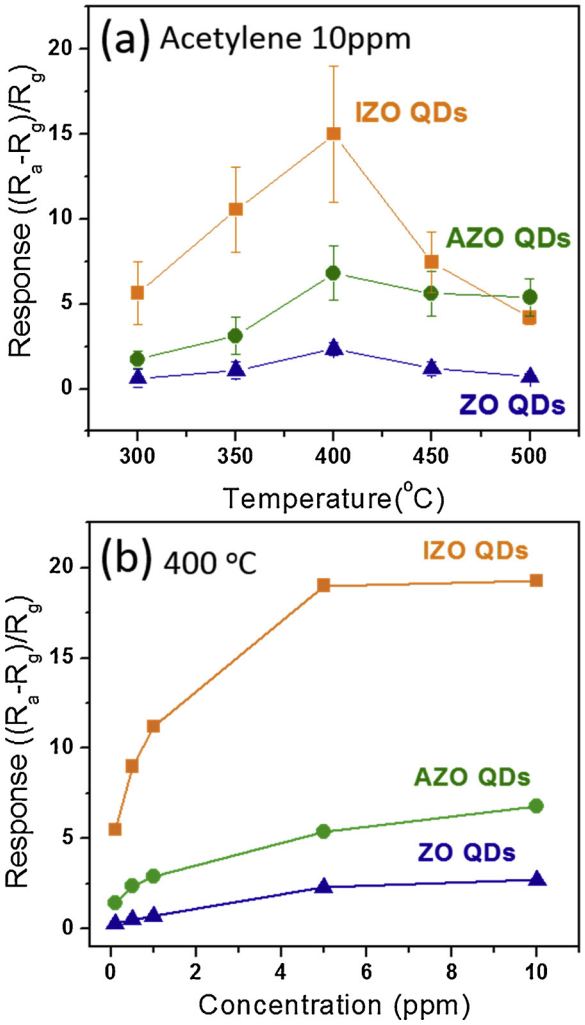

Fig. 4. Sensing responses of ZO (blue), AZO (green), and IZO QDs (green) as a function of operating temperature under exposure of 10 ppm acetylene (a) and as a function of acetylene concentration in the range of 0.1–10 ppm at their optimal working temperatures of 400 °C (b). (For interpretation of the references to colour in this figure legend, the reader is referred to the web version of this article).

confirms the wurtzite structure of the samples. The minimum of this peak differs slightly, for the IZO QDs it is ~468 cm^{-1}, for the AZO QDs ~462 cm^{-1}, and for the pristine ZO QDs ~456 cm^{-1}. The shifts of the peaks for IZO and AZO are likely related to the crystal perturbation caused by the change in bond length upon replacement of Zn with Al and In atoms in the lattice sites [30,34]. The larger shift of IZO is thus owing to the substitution of In^{3+}, which exhibits a larger ionic radius than Zn^{2+}. These results are consistent with the higher deterioration of crystallinity observed in IZO using XRD, and confirm that the doping elements Al and In were successfully incorporated into the Zn lattice sites.

The specific surface areas of the QD samples were estimated by the nitrogen adsorption–desorption method. Fig. 3 shows the N_2 adsorption–desorption isotherm of the ZO, AZO, and IZO QDs. As can be seen in Fig. 3, all the samples exhibit type-IV physisorption isotherms and a type-H1 hysteresis loop according to the International Union of Pure and Applied Chemistry (IUPAC) classification [37]. These types of isotherm curves are closely related to mesoporous materials. In particular, type H1 is often associated with porous materials that consist of agglomerates or compacts of approximately uniform spheres in a fairly regular array [37]. Therefore, the narrow hysteresis of the adsorption–desorption isotherm curves observed in the ZO, AZO, and IZO QD samples can be attributed to the mesoporous structures resulting from particle agglomeration. The Brunauer–Emmett–Teller (BET) specific surface areas of the nanoparticles were estimated from the N_2 adsorption branches as ~46.6, ~48.2, and 50.5 m^2/g for the ZnO, AZO, and IZO QDs, respectively. The surface area increases in order of pure ZO, AZO, and IZO QDs owing to the decrease in the particle size, as discussed with regard to the TEM and XRD data in Fig. 1.

In order to investigate the sensing properties of the ZO, AZO and IZO QDs upon exposure to acetylene, we measured their sensing responses at different operating temperatures (300–500 °C) and concentrations (0.1–10 ppm). The sensing response for the acetylene gas was obtained with a definition as $\Delta R/R_g$, where $\Delta R = (R_a - R_g)$, and R_g and R_a are the sensor resistances in environments acetylene and plain air, respectively. Fig. 4(a) shows the sensing response of the samples to 10 ppm of acetylene as a function of operating temperature. For all samples, the sensing response to 10 ppm acetylene was highest at a working temperature of 400 °C, i.e. ~3 for ZO, ~7 for AZO, and ~19 for IZO QDs (Fig. 4(a)). Fig. 4(b) shows the maximum sensing response of the samples to different acetylene concentrations at the optimal working temperature of 400 °C. We observed an increase in the sensing response with increasing acetylene concentration for all samples. The doped IZO and AZO QDs revealed an improved sensing performance compared to the undoped ZO QDs. In particular, the sensing response of IZO QDs was significantly enhanced at 10 ppm acetylene exposures. In

Table 1
Comparison of the acetylene sensing performance of various types of metal oxide-based sensors.

Sensing materials	Operating temperature [°C]	Acetylene concentration [ppm]	Response (R_a/R_g)	Sensitivity* [ppm^{-1}]	Detection limit [ppm]	Ref.
In-doped ZO QDs	400	10	19.3	~ 1.92	0.1	This work
Al-doped ZO QDs	400	10	6.8	~ 0.68	0.1	This work
ZnO QDs	400	10	2.7	~ 0.27	0.1	This work
Ni-doped ZnO NFs	250	2000	17.0	~ 0.01	1	[14]
NiO/SnO_2 heterostructures	206	100	12.8	~ 0.13	1	[15]
Ag/ZnO Hrc-rGO hybrid	200	100	11.3	~ 0.11	3	[16]
Ag/ vertical ZnO NR	200	1000	26.2	~ 0.03		[17]
Ag-SnO_2/rGO nanaocomposite film	90	10	8.0	~ 0.80		[18]
Pt/ZnO thick film	300	50	0.1		50	[19]

* sensitivity = response/concentration.

comparison to metal oxide-based gas sensors as previously reported [14–19], the acetylene sensing performance of IZO QDs are superior in terms of sensitivity and detection limit (Table 1).

In order to understand the doping effect on the differing sensing performances of AZO and IZO QDs, we investigated their chemical and electronic characteristics, such as oxygen vacancies and band gap. To analyze the surface composition and chemical state of the ZO, AZO, and IZO QD samples, we carried out an XPS analysis. In Fig. 5(a), the Zn 2p spectra of all samples show two main peaks located at ~1021 eV and ~1044 eV, corresponding to the Zn $2p_{3/2}$ and Zn $2p_{1/2}$ spin orbit, respectively. This implies the existence of a divalent oxidation state in the samples [29,38]. The Zn 2p spectra of the doped AZO and IZO QDs show a slight chemical shift in the binding energy in comparison to the undoped ZO QDs. This is likely due to the presence of Al and In dopants in the ZnO structures [29,39]. In Fig. 5(b), the Al 2p spectra show a peak only for the AZO QDs at a binding energy of ~74.7 eV, which is attributed to the Al–O bond, as the Al^{3+} ion is substituted into the Zn^{2+} ion sites in the ZnO lattice [29,38]. This binding energy is different from that in the cases of metallic Al (Al 2p: 72.8 eV) [40] and Al_2O_3 (Al 2p: 75.6 eV) [41]. In Fig. 5(c), two main peaks of In $3d_{5/2}$ at ~444.2 eV and In $3d_{3/2}$ ~451.8 eV [39,42] are exhibited only in the IZO QDs. This is due to the presence of In dopant as In^{3+} ion in the ZnO crystal [39,42]. Accordingly, the results of the Al 2p and In 3d spectra indicate the successful incorporation of Al and In into the Zn^{2+} sites of ZnO. This is in good agreement with the peak shifts in the XRD patterns shown in Fig. 1(b).

To analyze the oxidation states of the elements present in the ZO, AZO, and IZO QDs, we carried out detailed analysis of the XPS O 1s spectra. The XPS spectra of the O 1s state of ZO (Fig. 5(d)), AZO (Fig. 5(e)) and IZO QDs (Fig. 5(f)) were each deconvoluted into three quasi-Gaussian peaks centered at about 530, 531, and 532 eV. The peak at ~529.8 eV (red line) corresponds to the O^{2-} ions in the Zn-O bonds of the ZnO structure [29]. The peak at ~531.2 eV (orange line) is associated with adsorbed oxygen ions (O^- and O^{2-}). These significantly influence the gas-sensing performances in the oxygen-deficient regions within ZnO QDs, such as oxygen vacancies and oxygen interstices [29]. Because the peak intensities differ among the samples, we expect the concentrations of the oxygen deficiencies to vary as well. By

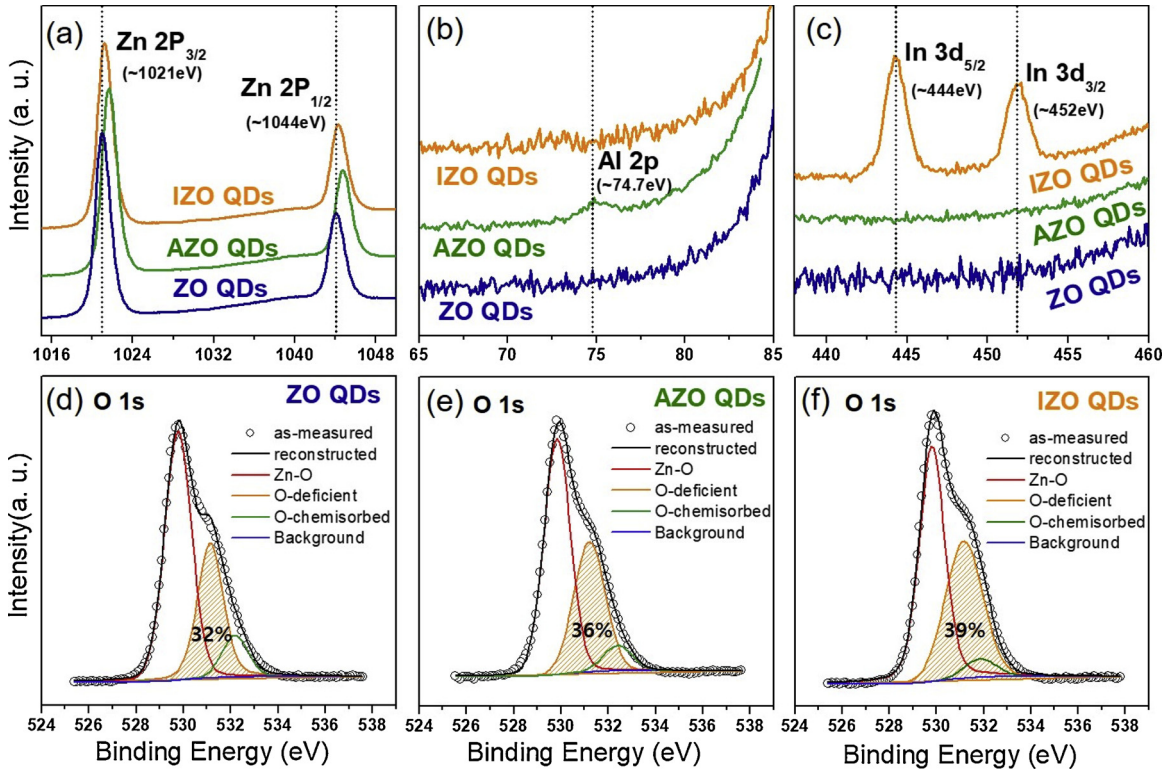

Fig. 5. XPS spectra of (a) Zn 2p, (b) Al 2p, and (c) Id 3d of ZO (blue), AZO (green) and IZO QDs (orange), and O 1 s XPS spectra of (d) ZO, (e) AZO, and (f) IZO QDs. (For interpretation of the references to colour in this figure legend, the reader is referred to the web version of this article).

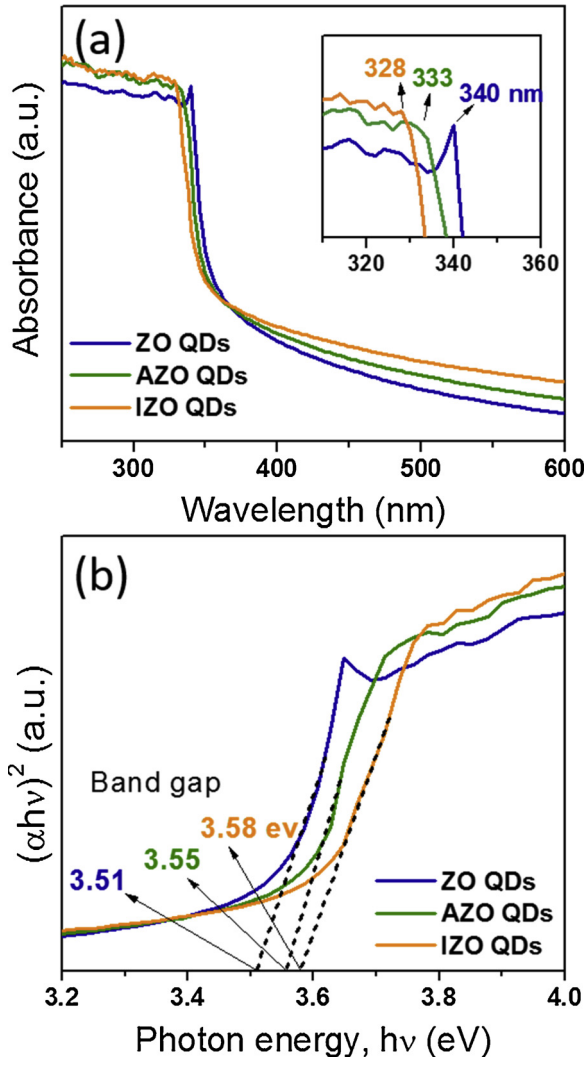

Fig. 6. UV–vis absorption spectra (a) and optical band gap energies (b) of ZO (blue), AZO (green), and IZO QDs (orange). The inset shows a zoom into the absorption peak/edge. (For interpretation of the references to colour in this figure legend, the reader is referred to the web version of this article).

determining the area fraction of this oxygen-deficient peak in the deconvoluted O 1s spectra, we were able to estimate the concentrations of the oxygen deficiencies to about 32, 36, and 39% for ZO, AZO, and IZO QDs, respectively. The results reveal that the doped IZO and AZO QDs contain more oxygen vacancies than the undoped ZO QDs. The In dopant was found to provide more oxygen vacancies in ZnO than Al. This can be attributed to the loss of crystallinity when In^{+3} is substituted, which may lead to more defects such as oxygen deficiencies. The peak at ~532.2 eV (green line) is attributed to chemisorbed oxygen species, such as H_2O, O_2, and $-CO_3$ adsorbed on the surface of ZnO [29].

In order to analyze the optical band gap energy of the samples, we performed UV–vis spectroscopy. We observed a relatively sharp absorption peak at ~340 nm for the undoped ZO QDs (Fig. 6(a)). The absorption edges of AZO and IZO were instead found to shift towards higher energies, i.e. lower wavelengths of ~333 nm and ~328 nm, respectively. This was accompanied by a broadening of the peak. Based on the UV–vis spectra we determined the optical band gap energy (E_g) of the QDs using the Tauc relation [43]:

$$\alpha h\nu = C(h\nu - E_g)^n \quad (1)$$

where α is the absorption coefficient, C is a constant, hν is the energy of the incident photons, n = 1/2 for direct band gap semiconductors, and E_g is the optical band gap. More specifically, the optical band gap energy was calculated by extrapolating the function $[F(\alpha h\nu)^2]$ versus hν to zero [44]. We found the optical band gap of the samples to vary from ~3.51 eV for the undoped ZO QDs to ~3.55 eV for AZO QDs and ~3.58 eV for IZO QDs (Fig. 6(b)).

The band gap is expected to depend on several factors such as carrier concentration, lattice strain and size effect [45]. The blue shift in band gap energy for the doped samples can mainly be explained by the Burstein-Moss effect [46]. The donor Al and In atoms provide additional carriers, which cause to the Fermi level to move into the conduction band, so that the energy gap becomes larger. In addition, the carrier concentration can be increased by an increase in oxygen vacancies [47]. As observed using XPS, the doped samples have a larger amount of oxygen vacancies than the undoped sample. Therefore, the carrier concentration of the doped samples becomes larger than that of the undoped sample. Moreover, the increase in band gap for the doped samples compared to the undoped sample can be attributed to the decrease in particle size [48–51]. Similarly, the larger band gap of the IZO QDs as compared to the AZO QDs can be attributed to the increased carrier concentration and smaller particle size of IZO QDs.

According to the sensing mechanism of a ZnO-based sensor [24], a higher sensing performance is closely related to an increase in the depletion layer thickness at the initial state. This results in a greater number of reactive sites for the target gas. The IZO QDs, which in our study demonstrate the best sensing performance, exhibit indeed a thicker depletion layer than the AZO QDs. This is owing to the increased number of oxygen vacancies, which result in a larger carrier concentration. In addition, the IZO QDs possess a greater number of reactive sites for detecting acetylene because of the smaller particles sizes.

For real applications, we tested the repeatability, humidity interference, and long-term stability of the IZO QDs toward 10 ppm acetylene at the optimal working temperature of 400 °C. Fig. 7(a) shows the reproducibility of the sensing resistance of IZO QDs for 10 ppm acetylene for 13 cycles at 400 °C. Fig. 7(b)–(d) present the resistance curves for the 4^{th}, 5^{th}, and 12^{th} cycles, respectively. The resistance curves exhibited high noise, which can be attributed to the low concentration of QD particles in the IZO QD sensor. It is very difficult to ensure that the concentration of the loaded QD particles is constant by using a dropping method, but this will be studied further. However, Fig. 7(a)–(d) clearly show that the sensing resistance is nearly stable and constant throughout 13 cycles of gas input and release, which indicates good repeatability in the response of IZO QDs for 10 ppm acetylene.

Fig. 7(e) shows the variation in the sensor response of IZO QDs to 10 ppm acetylene under different humid conditions (0–90 RH%) at the optimal working temperature of 400 °C. As the relative humidity increases, the response decreases: there was a ~50% reduction in response to 10 ppm acetylene at 90 RH%. This indicates that the sensing performance of IZO QDs at high humidity is significantly degraded by the contamination of their reactive sites due to the adsorption of water molecules. However, if the IZO QD sensor is adopted in GC-based online DGA using a membrane-based gas-extraction method, the effect of humidity on the sampling gas extracted from the transformer oil can be significantly reduced.

Further, Fig. 7(f) shows a long-term stability test of the IZO QDs when exposed to 10 ppm acetylene at the optimal working temperature of 400 °C, which was measured at an interval of 5 or 10 days for 60 days. As a result, the response decreased by ~50% on the 20^{th} day, and after 50 days, the response decreased by ~65%, reaching saturation within the error range. The reduced response during long-time continuous measurements can be attributed to the contamination of reactive sites on the IZO QD surface. The smaller the particles, the better their sensing reactivity, but the more likely they are to become contaminated. Therefore, further study is needed to solve the long-term stability problem of QD samples. However, it is noted that the response

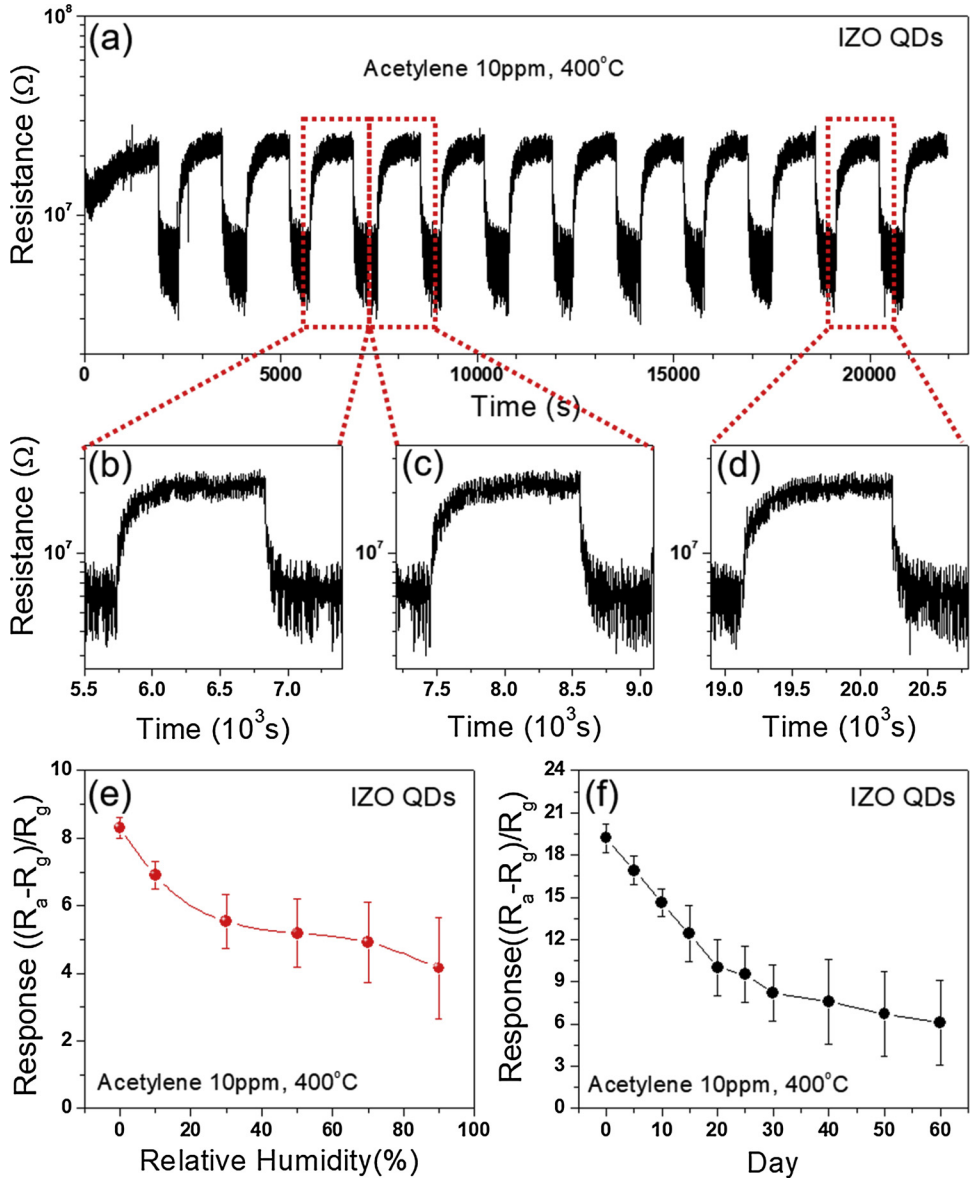

Fig. 7. (a) Reliability of IZO QDs in sensing 10 ppm acetylene over 13 cycles at 400 °C; (b)-(d) sensing resistance curves for the 4th, 5th, and 12th cycles; (e) variation in the response of IZO QDs for 10 ppm acetylene as a function of relative humidity at 400 °C; (f) a long-term stability test of IZO QDs exposed to 10 ppm acetylene at 400 °C measured at an interval of 5 or 10 days for 60 days.

of ~6 after 60 days is still higher than that reported in other metal oxide-based gas sensors (Table 1).

To test the sensitivity of the IZO QDs for acetylene detection based on GC technology, we used our recently developed mini-GC. Using the mini-GC, we recorded a sensor signal of the QDs in acetylene/air mixtures with varying acetylene concentrations (5–1000 ppm) at the optimal working temperature of each sample. i.e. 450 °C for ZO, 350 °C for AZO, and 350 °C for IZO. The Δ sensor signal was defined as the logarithmic difference in the sensor resistances in air and under exposure of the acetylene/air gas mixture:

$$\Delta \text{ sensor signal} = \log(\text{resistance})_{max} - \log(\text{resistance})_{min} \quad (2)$$

where $\log(\text{resistance})_{max}$ denotes the maximum resistance before the sensor was exposed to the target gas; and $\log(\text{resistance})_{min}$ the minimum resistance during the exposure [26,27]. We observed that the chromatograms of the air/acetylene gas mixtures exhibit a single peak at ~ 169 s for ZO (Fig. 8(a)), ~ 146 s for AZO (Fig. 8(b)), and ~ 100 s for IZO (Fig. 8(c)), which corresponds to the detection of acetylene. This means that acetylene was detected most rapidly by the IZO QDs. In order to estimate the detection limit of the various QDs for acetylene, we plotted the peak height value (Δ sensor signal) as a variation of acetylene concentration. The sensing responses (Δ sensor signal) to 1000 ppm acetylene were found to be ~0.19 for ZO, ~0.37 for AZO, and ~0.71 for IZO (Fig. 8(d)). The lowest detection limits of ZO, AZO, and IZO QDs were estimated to be 1000, 500, and 10 ppm, respectively. Thus, the IZO QDs show the best response signal, detection time and detection limit of all tested samples in the mini-GC device. Its sensing response to 10 ppm acetylene of ~19 was, however, lower than that of undoped ZnO QDs to other target gases, e.g. ~1500 to 10 ppm acetone [26], ~4614 to 20 ppm 2-chloroethyl ethyl sulfide (2-CEES) [27], and ~42 to 1 ppm isoprene [28]. Nevertheless, the mini-GC integrated with an IZO QDs-based sensor is able to selectively detect 10 ppm acetylene gas in an air environment.

We tested the sensing ability of the IZO QDs incorporated into the mini-GC device for detection of i) other fault gases, ii) other reducing gases, and iii) acetylene mixed with other fault gases in an air-balanced gas at the optimal operating temperature (350 °C) of the device. Fig. 9 shows the variations in the sensor signal of the mini-GC integrated with

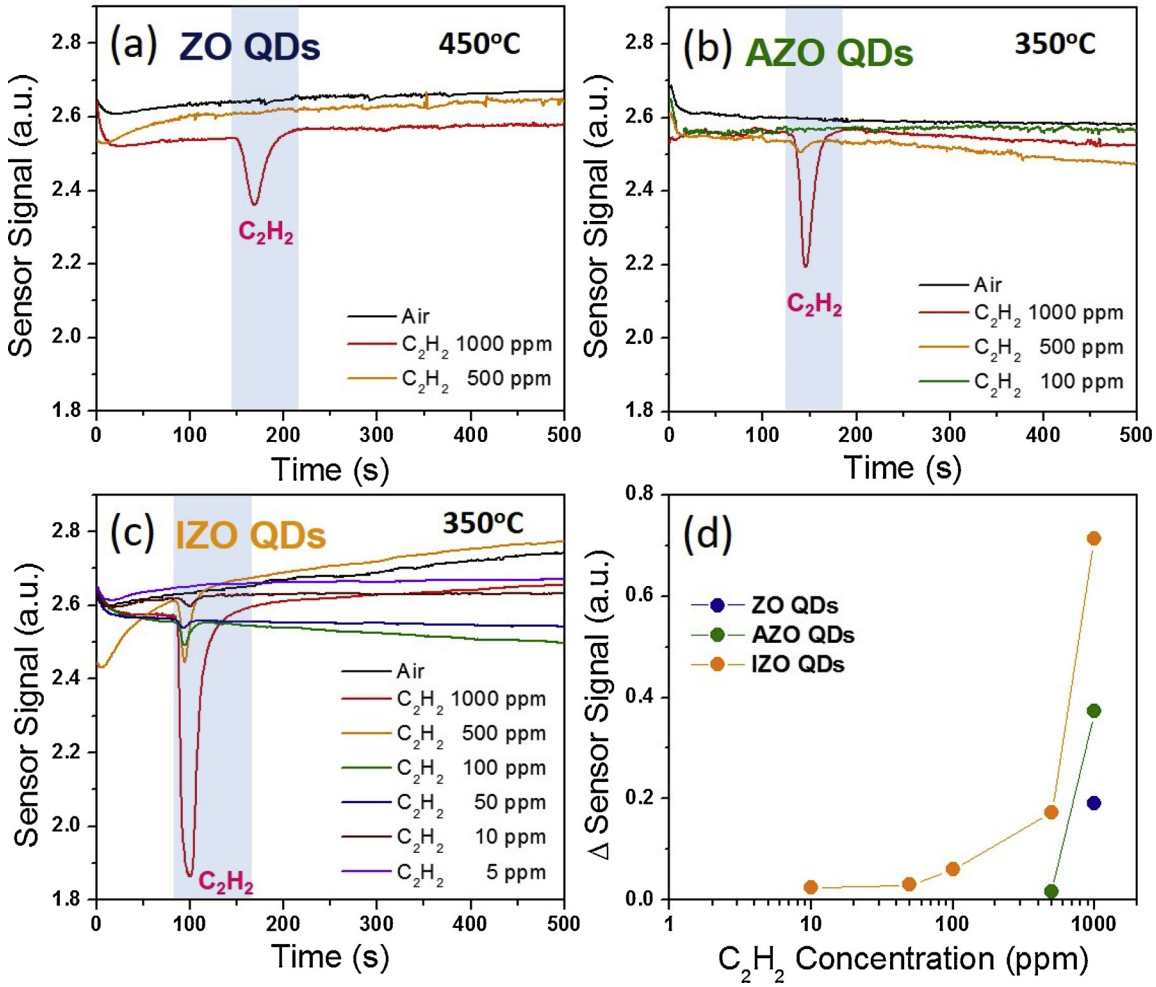

Fig. 8. Sensor signals as measured in a miniaturized gas chromatographic column (mini-GC) integrated with (a) ZO, (b) AZO, and (c) IZO QDs sensors for various acetylene concentrations (5–1000 ppm) at their optimal working temperatures of 450 °C, 350 °C, and 350 °C, respectively; (d) Peak height of the Δ sensor signal at various acetylene concentrations (10–1000 ppm) for ZO (blue), AZO (green) and IZO (orange) QDs.

the IZO QDs for the various target gases. For the test of case i), 100 ppm H_2, 20 ppm C_2H_2, 10 ppm CH_4, 10 ppm CO, and 0.1% CO_2 are exposed. For the test of case ii), 10 ppm NO, 10 ppm NH_3, and 10 ppm C_2H_5OH are exposed. For the test of case iii), 50 ppm C_2H_2 mixed with 500 ppm H_2 are exposed.

The chromatograms of the different gases are compared with those of air (Fig. 9(a)) and N_2 (Fig. 9(b)). As shown in Fig. 9(b) and (c), the peaks corresponding to the detection of N_2 and H_2 (100 ppm H_2 in synthetic air) appear near 21 s. The N_2 sensing of the IZO QDs can be attributed to the reduction of adsorbed oxygen ions on the surface of the IZO QDs. When the unreactive N_2 gas is injected into the sensor as a target gas, the N_2 concentration increases instantaneously and the adsorbed oxygen ion concentration decreases. This results in a decrease in resistance. For 20 ppm C_2H_2 in synthetic air, only one peak, indicating the detection of acetylene, was observed at ~105 s (Fig. 9(d)). However, except for the N_2 peak, there was no indication of the detection of the other fault gases, such as 10 ppm CH_4 (Fig. 9(e)), 10 ppm CO (Fig. 9(f)), and 0.1% CO_2 (Fig. 9(g)). The sensing results in Figs. 9(c)–9(g) indicate that the mini-GC integrated with the IZO QDs can detect only H_2 and C_2H_2 among the various fault gases. For the tests of other reducing gases of 10 ppm NO, 10 ppm NH_3, and 10 ppm C_2H_5OH, only 10 ppm C_2H_5OH was detectable at approximately 43 s, as shown in Fig. 9(h)–(j). This provides a notable feature that this device can be utilized as an alcohol sensor. For 50 ppm C_2H_2 mixed with 500 ppm H_2, two peaks are observed at 21 s and 105 s, corresponding to hydrogen and acetylene gas, respectively (Fig. 9(k)). Thus, we confirmed that the major fault gases of H_2 and C_2H_2 can be separately detected from other gases within ~100 s by using mini-GC integrated with the IZO QDs.

4. Conclusion

We investigated the doping effect on the sensing properties of various ZnO QDs for the detection of acetylene. Undoped ZO QDs and doped AZO and IZO QDs were prepared by a wet chemical method. Using TEM, XRD, and FTIR analyses, we found that the prepared ZnO QDs exhibited different particle sizes (> 5 nm for ZO, ~4 nm for AZO, and ~3.6 nm for IZO) and that the doping elements Al and In were successfully incorporated into the Zn lattice sites. The IZO QDs exhibited a better sensing performance for 10 ppm acetylene than ZO and AZO QDs. The maximum sensing response was ~19 for IZO, ~7 for AZO, and ~3 for ZO at their optimal working temperature of 400 °C. Using XPS and UV–vis spectroscopy, we discovered that the higher sensing response of IZO QDs can be attributed to a greater number of reactive sites for detecting acetylene, which likely originates from an increased number of oxygen vacancies, a larger optical band gap, and a larger surface area of IZO compared to ZO and AZO QDs. The sensitivity of IZO to acetylene was found to be superior to that of other previously reported acetylene sensors based on semiconducting metal oxides. We also achieved the selective detection of 10 ppm acetylene in air using an IZO QD sensor incorporated into a miniaturized gas chromatography setup (mini-GC) that was recently developed by our group.

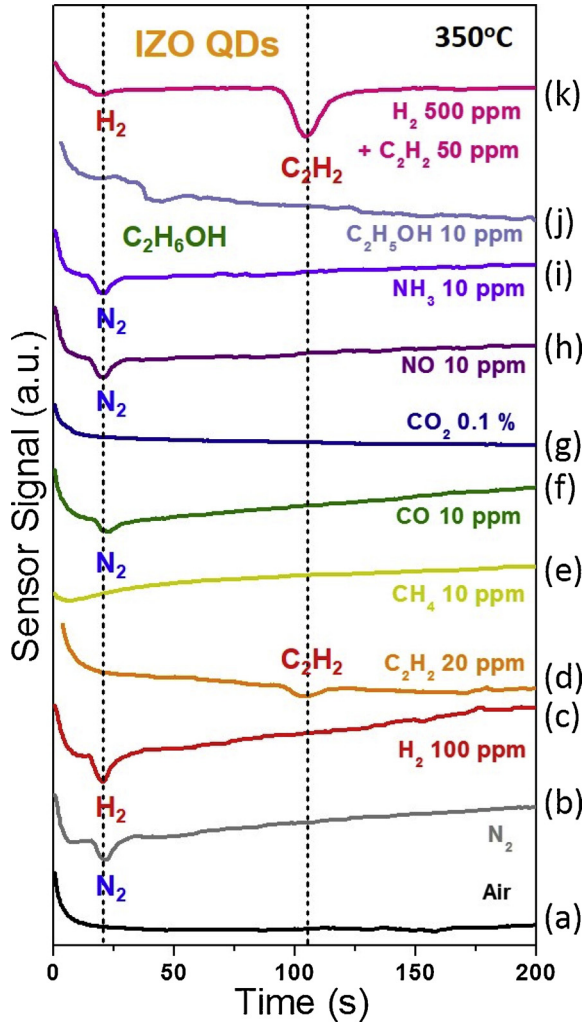

Fig. 9. Sensor signals of the mini-GC integrated with the IZO QD sensor for (a) synthetic air, (b) nitrogen, and five different types of fault gases ((c) 100 ppm H_2, (d) 20 ppm C_2H_2, (e) 10 ppm CH_4, (f) 10 ppm CO, and (g) 0.1% CO_2), three different types of reducing gases ((h) 10 ppm NO, (i) 10 ppm NH_3, and (j) 10 ppm C_2H_5OH), and (k) 50 ppm C_2H_2 mixed with 500 ppm H_2 tested at 350 °C.

Furthermore, we found that the device can detect the major fault gases of hydrogen and acetylene separately. Our study demonstrates that the mini-GC device integrated with the IZO QDs can be utilized in the GC-based on-line DGA. This device makes it possible to detect small amounts of acetylene gas in transformer oils, which can be used to diagnose transformer failure in near future.

Acknowledgements

This research was supported by the Priority Research Centers Program through the National Research Foundation of Korea (NRF) (2019R1A6A1A11055660), and the Medium and Large Complex Technology Commercialization Project through the Commercialization Promotion Agency for R&D Outcomes (2019K000045). Both were funded by the Korea government (the Ministry of Science, ICT and Future Planning).

References

[1] M. Duval, A review of faults detectable by gas-in-oil analysis in transformers, IEEE Electr. Insul. Mag. 18 (2002) 8–17.
[2] M. Wang, A.J. Vandermaar, K.D. Srivastava, Review of condition assessment of power transformers in service, IEEE Electr. Insul. Mag. 18 (2002) 12–25.
[3] M. Duval, J. Dukarm, Improving the reliability of transformer gas-in-oil diagnosis, IEEE Electr. Insul. Mag. 21 (2005) 21–27.
[4] J. Faiz, M. Soleimani, Dissolved gas analysis evaluation in electric power transformers using conventional methods a review, IEEE Trans. Dielectr. Electr. Insul. 24 (2017) 1239–1248.
[5] J. Ding, X. Li, J. Cao, L. Sheng, L. Yin, X. Xu, New sensor for gases dissolved in transformer oil based on solid oxide fuel cell, Sens. Actuators B Chem. 202 (2014) 232–239.
[6] F. Wan, et al., Using a sensitive optical system to analyze gases dissolved in samples extracted from transformer oil, IEEE Electr. Insul. Mag. 30 (2014) 15–22.
[7] K. Nagapriya, et al., Laser calorimetry spectroscopy for ppm-level dissolved gas detection and analysis, Sci. Rep. 7 (2017) 42917.
[8] W. Chen, B. Liu, H. Zhou, Y. Wang, C. Wang, Diode laser-based photoacoustic spectroscopy detection of acetylene gas and its quantitative analysis, Eur. Trans. Electr. Power 22 (2012) 226–234.
[9] G. Yan, A.P. Zhang, G. Ma, B. Wang, B. Kim, J. Im, S. He, Y. Chung, Fiber-optic acetylene gas sensor based on microstructured optical fiber bragg gratings, IEEE Photonics Technol. Lett. 23 (2011) 1588–1590.
[10] G. Ma, S. Zhao, J. Jiang, H. Song, C. Li, Y. Luo, H. Wu, Tracing acetylene dissolved in transformer Oil by tunable diode laser absorption spectrum, Sci. Rep. 7 (2017) 14961.
[11] H. Tsukioka, K. Sugawara, Apparatus for continuously monitoring hydrogen gas dissolved in transformer oil, IEEE Trans. Dielectr. Electr. Insul. E1-16 (6) (1981) 502–509.
[12] L. Tong, G. Wu, J. Sheng, J. Zhang, L. Zhou, Oil-gas separation mechanism of polymer membranes applied to on-line transformer dissolved gases monitoring, IEEE International Symposium on Electrical Insulation, (2004), pp. 19–22.
[13] S. Liu, L.-C. Ma, C.-H. Chen, C. Chen, Y.S. Lin, Highly gas permeable, ultrathin Teflon AF2400/γ-alumina composite hollow fiber membranes for dissolved gas analysis, J. Memb. Sci. 540 (2017) 243–250.
[14] X. Wang, M. Zhao, F. Liu, J. Jia, X. Li, L. Cao, C_2H_2 gas sensor based on Ni-doped ZnO electrospun nanofibers, Ceram. Int. 39 (2013) 2883–2887.
[15] Y. Lin, C. Li, W. Wei, Y. Li, S. Wen, D. Sun, Y. Chen, S. Ruan, A new type of acetylene gas sensor based on a hollow heterostructure, RSC Adv. 5 (2015) 61521–61527.
[16] A.S.M. Iftekhar Uddin, D.T. Phan, G.S. Chung, Low Temperature acetylene gas sensor based on Ag nanoparticles-loaded ZnO-reduced graphene oxide hybrid, Sens. Actuators B Chem. 207 (2015) 362–369.
[17] A.S.M. Iftekhar Uddin, U. Yaqoob, G.S. Chung, A novel flexible acetylene gas sensor based on PI/PTFE-supported Ag-loaded vertical ZnO nanorods array, Sens. Actuators B Chem. 222 (2016) 536–543.
[18] L. Jin, W. Chen, Q. Zhou, G. Xiao, C. Yu, Detection of acetylene dissolved in transformer oil using SnO2/rGO nanocomposite gas sensor, IEEE POWERCON (2016) No. 7754032.
[19] N. Tanmaekong, C. Liewhiran, A. Wisitsoraat, S. Phanichphant, Acetylene sensor based on Pt/ZnO Thick films as prepared by flame spray pyrolysis, Sens. Actuators B Chem. 152 (2011) 155–161.
[20] M. Righettoni, A. Amann, S.E. Pratsinis, Breath analysis by nanostructured metal oxides as chemo-resistive gas sensors, Mater. Today 18 (2015) 163–171.
[21] M.H. Darvishnejad, A.A. Firooz, J. Beheshtian, A.A. Khodadadi, Highly sensitive and selective ethanol and acetone gas sensors by adding some dopants (Mn, Fe, Co, Ni) onto hexagonal ZnO plates, RSC Adv. 6 (2016) 7838–7845.
[22] R. Yoo, D.M. Lee, S.M. Cho, W.Y. Lee, Doping effect on the sensing properties of ZnO nanoparticles for detection of 2-chloroethyl ethylsulfide as a mustard simulant, Ran Sens. Actuators B: Chem. 254 (2018) 1242–1248.
[23] L. Wang, S. Wang, M. Xu, X. Hu, H. Zhang, Y. Wang, W. Huang, A Au-functionalized ZnO nanowire gas sensor for detection of benzene and toluene, Phys. Chem. Chem. Phys. 15 (2013) 17179–17186.
[24] A. Koo, R. Yoo, S.P. Woo, H.-S. Lee, W. Lee, Enhanced acetone-sensing properties of Pt-decorated Al-doped ZnO nanoparticles, Sens. Actuators B Chem. 280 (2019) 109–119.
[25] S. Bai, J. Hu, D. Li, R. Luo, A. Chen, C.C. Liu, Quantum-sized ZnO nanoparticles: synthesis, characterization and sensing properties for NO2, J. Mater. Chem. 21 (2011) 12288–12294.
[26] H. Jung, W. Cho, R. Yoo, H.-S. Lee, Y.-S. Choe, J.Y. Jeon, W. Lee, Highly selective real-time detection of breath acetone by using ZnO quantum dots with a miniaturized gas chromatographic column, Sens. Actuators B Chem. 274 (2018) 527–532.
[27] J.H. Lee, H. Jung, R. Yoo, Y. Park, H.-S. Lee, Y.-S. Choe, W. Lee, Real-time selective detection of 2-chloroethyl ethyl sulfide (2-CEES) using an Al-doped ZnO quantum dot sensor coupled with a packed column for gas chromatography, Sens. Actuators B Chem. 284 (2019) 444–450.
[28] Y. Park, R. Yoo, S. Park, J.H. Lee, H. Jung, H.-S. Lee, W. Lee, Highly sensitive and selective isoprene sensing performance of ZnO quantum dots for a breath analyzer, Sens. Actuators B Chem. 290 (2019) 258–266.
[29] R. Sankar Ganesh, M. Navaneethan, G.K. Mani, S. Ponnusamy, K. Tsuchiya, C. Muthamizhchelvan, S. Kawasaki, Y. Hayakawa, Influence of Al doping on the structural, morphological, optical, and gas sensing properties of ZnO nanorods, J. Alloys. Compd. 698 (2017) 555–564.
[30] A.N. Mallikan, A. Ramachandra Reddy, K. SowriBabu, K. Venugopal Reddy, Synthesis and optical characterization of aluminum doped ZnO nanoparticles, Ceram. Int. 40 (2014) 12171–12177.
[31] K.U. Sim, S.W. Shin, A.V. Moholkar, J.H. Yun, J.H. Moon, J.H. Kim, Effects of dopant (Al, Ga, and In) on the characteristics of ZnO thin films prepared by RF magnetron sputtering system, Curr. Appl. Phys. 10 (2010) S463–S467.
[32] B. Paul, B. Singh, S. Ghosh, A. Roy, A comparative study on electrical and optical

properties of group III (Al, Ga, In) doped ZnO, Thin Solid Films 603 (2016) 21–28.
[33] X.-Y. Feng, Z. Wang, C.-W. Zhang, P.-J. Wang, Electronic structure and energy band of IIIA doped group ZnO nanosheets, J. Nanomater. (2013) Article ID 181979.
[34] N. Rajeshwari, Y.A. Chandra Bose, Absorption-emission study of hydrothermally grown Al:ZnO nanostructures, J. Alloys. Compd. 509 (2011) 8493–8500.
[35] I. Khan, S. Kahn, R. Nongjai, H. Ahmed, W. Khan, Structural and optical properties of gel-combustion synthesized Zr doped ZnO nanoparticles, Opt. Mater. 35 (2013) 1189–1193.
[36] S.S. Alias, A.B. Ismail, A.A. Mohamad, Effect of pH on ZnO nanoparticle properties synthesized by sol–gel centrifugation, J. Alloys. Compd. 499 (2010) 231–237.
[37] K.S.W. Sing, D.H. Everett, R.A.W. Haul, L. Moscou, R.A. Pierotti, J. Rouquérol, T. Siemieniewka, Reporting physisorption data for gas/solid systems with special reference to the determination of surface area and porosity, Pure Appl. Chem. 57 (1985) 603–619.
[38] J.T. Chen, J. Wang, R.F. Zhuo, D. Yan, J.J. Feng, F. Zhang, P.X. Yan, Appl. Surf. Sci. 255 (2009) 3959–3964.
[39] Z. Zhu, B. Li, J. Wen, Z. Chen, Z. Chen, R. Zhang, S. Ye, G. Fang, J. Qian, Indium-doped ZnO horizontal nanorods for high on-current field effect transistors, RSC Adv. 7 (2017) 54928–54933.
[40] R. Hauert, J. Patscheider, M. Tobler, R. Zehringe, Surf. Sci. 292 (1993) 121–129.
[41] M. Kundu, N. Miyata, M. Ichikawa, Study of ultrathin Al_2O_3/Si(001) interfaces by using scanning reflection electron microscopy and x-ray photoelectron spectroscopy, Appl. Phys. Lett. 78 (2001) 1517–1519.
[42] B.L. Zhu, D.W. Zeng, J. Wu, W.L. Song, C.S. Xie, Synthesis and gas sensitivity of In-doped ZnO nanoparticles, J. Mater. Sci. Mater. Electron. 14 (2003) 521–526.
[43] J. Tauc, Amorphous and Liquid Semiconductors, Plenum Press, New York, 1975, p. 171.
[44] R.S. Weber, Effect of local structure on the UV-Visible absorption edges of molybdenum oxide clusters and supported molybdenum oxides, J. Catal. 151 (1995) 470–474.
[45] S. Husain, L.A. Alkhtaby, E. Giorgetti, A. Zoppi, M.M. Miranda, Effect of Mn doping on structural and optical properties of solgel derived ZnO nanoparticles, J. Lumin. 145 (2014) 132–137.
[46] B.E. Sernelius, K.F. Berggren, Z.C. Jin, I. Hamberg, C.G. Granqvist, P Band-gap tailoring of ZnO by means of heavy Al doping, Phys. Rev. B 37 (1988) 10244–10248.
[47] C.E. Kim, P. Moon, S. Kim, J.-M. Myoung, H.W. Jang, J. Bang, I. Yun, Effect of carrier concentration on optical bandgap shift in ZnO:Ga thin films, Thin Solid Films 518 (2010) 6304–6307.
[48] A.L. Efros, Interband absorption of light in a semiconductor sphere, Sov. Phys. Semicond. 16 (1982) 772.
[49] K.F. Lin, H.M. Cheng, H.C. Hsu, L.J. Lin, W.F. Hsieh, Band gap variation of size-controlled ZnO quantum dots synthesized by sol–gel method, Chem. Phys. Lett. 409 (2005) 208–211.
[50] M.B. Sahana, C. Sudakar, G. Setzler, A. Dixit, J.S. Thakur, G. Lawes, R. Naik, V.M. Naik, P.P. Vaishnava, Bandgap engineering by tuning particle size and crystallinity of SnO_2–Fe_2O_3 nanocrystalline composite thin films, Appl. Phys. Lett. 93 (2008) 231909.
[51] W. Han, J. Kim, H.H. Park, Control of electrical conductivity of highly stacked zinc oxide nanocrystals by ultraviolet treatment, Sci. Rep. 9 (2019) 6244.

Min Sun Park received a Bachelor's degree in Chemistry at Sungkyunkwan University in 2017. Since 2017, she has been studying the development of breath analyzers and miniaturized GC integrated with metal oxide-based gas sensors as a Master's student at Yonsei University.

Jun Ho Lee received a Bachelor's degree and a Master's degree in Material Science and Engineering at Seoul National University in 2015 and 2017, respectively. Since 2017, he has been working on developing a miniaturized GC that is integrated with a metal oxide-based gas sensor as a researcher at Yonsei University.

Yunji Park received a Bachelor's degree in Chemistry at Kyunghee University in 2016. She received a Master's degree in Material Science and Engineering at Yonsei University for the study on a breath analyzer using metal oxide-based gas sensors. She joined Samsung Electronics in 2018.

Ran Yoo received a Ph.D. degree in Materials Science and Engineering at Yonsei University in 2018. Her research interest was in various nanostructured materials related to chemiresistive gas sensors based on metal oxide semiconductors. She joined the Korea Institute of Energy Research in 2018.

Seungryol Park is currently a team leader of the LG Display's LC Development Team. He received a Master's degree in Material Science and Engineering at Yonsei University in 2009. Since 2015, he has been studying various nanostructured materials related to chemiresistive gas sensors based on metal oxide semiconductors as a doctoral student at Yonsei University.

Hwaebong Jung received a Ph.D. degree in Materials Science and Engineering at Yonsei University in 2019. His research interests are in nanomaterial-based gas sensors and a breath analyzer using metal oxide gas sensors.

Wonkung Kim received a Ph.D. degree in Material Science and Engineering at Yonsei University in 2018. He is currently an adjunct professor in the School of Nano & Materials Science and Engineering at Kyungpook National University. In recent years, his research interests have focused on metal oxide gas sensors.

Hyun-Sook Lee received a Ph.D. degree in Physics at POSTECH in 2008. Since 2015, she has been working as a research professor in the Department of Materials Science and Engineering atYonsei University. Her research interests are in various materials related to high-temperature superconductors, solid-state hydrogen storages, rare-earth/rare-earth-free permanent magnets, and nanostructured metal oxide semiconductor gas sensors.

Wooyoung Lee is the Dean of School of Materials Science and Engineering and the Director of Institute of Nanoscience and Nanotechnology at Yonsei University in Korea. He received a BS degree in Metallurgical Engineering in 1986, a MS degree in Metallurgical Engineering from the Yonsei University in 1988. He received a Ph.D. degree in Physics from University of Cambridge, United Kingdom in 2000. He is a regular member of National Academy of Engineering of Korea. He was a member of National Science & Technology Council and a director in Korea Israel Industrial R&D Foundation. In recent years, his research interests have centered on hydrogen sensors, various metal oxide semiconducting gas sensors, and breath analyzers. He is also studying thermoelectric materials and devices, and permanent magnets. He has received a number of awards in nano-related research areas and a Service Merit Medal (2008) from the Government of Korea due to contribution on the development of intellectual properties. He has authored and co-authored over 200 publications, and has edited three special books on nano-structured materials and devices.